Integration and Testing of a Hydrogen Fuel Cell in a Hybrid Electric Propulsion System

Luís Miguel Martins Costa e Silva
luis.costa.silva@tecnico.ulisboa.pt

Instituto Superior Técnico, Lisboa, Portugal

December 2022

Abstract

With the increasing environmental concerns and regulations, the aviation sector strives to find more sustainable propulsion alternatives. Hybrid electric propulsion systems (HEPS) and hydrogen as a power source have been proposed as some potential solutions. This document reports the steps taken to study a hydrogen fuel cell (FC) as a power source for propulsion of unmanned aerial vehicles (UAVs). A proton exchange membrane FC system, with a 24-cell stack, was supplied with a compressed hydrogen gas cylinder, to generate electricity. Its two operation modes were tested to power several different electric motors (EMs), with particular emphasis on UAV applications. A parallel hybrid test bench, composed of two electric motors mechanically coupled, was used to compare the performance of the FC with Lithium-Polymer batteries. The performance metrics include the hybridization factor, different throttle signals and system loadings.
Keywords: hybrid electric propulsion, hydrogen fuel cell, unmanned aerial vehicles, proton exchange membrane fuel cell, parallel hybrid configuration

1. Introduction

As the years pass, climate change and greenhouse gases emissions increasingly become a more pressing issue. As public awareness towards the issue grows, and policies shift to more environmentally friendly ones, the industrial world has to adapt. The aviation industry is no exception in this need for change, and hybrid electric propulsion appears as part of the solution for this sector.

Globally, commercial aviation has experienced immense growth over the past decades, and it is expected to continue this path for the foreseeable future. Airbus estimates that, until the year 2040, the global need for new aircraft is nearly 40,000, with the total number of aircraft more than doubling [1]. This presents itself as one more contributing factor to the global impact of this fossil-fuel-heavy industry, and to counteract it, new configurations need to be developed and implemented.

The largest impact of aviation on the environment comes from atmospheric emissions of pollutant gases, in particular CO_2 and NO_X. Carbon dioxide emissions are one of the main source for human-made climate change, and the aviation sector contributes significantly to emissions: by 2010 it was the source of at least 3% of the total anthropogenic CO_2 emissions, showing a growth trend [2].

While the objective of the global research effort is the eventual application of more sustainable alternative propulsion systems in aircraft of all sizes, UAV are of particular interest, before scaling up, being a versatile and lower risk alternative to traditional aircraft. With the goal of reducing emissions and saving fuel, hybrid electric propulsion systems constitute an attractive option being studied. A HEPS aims to take advantage of the strong points of different traditional propulsion systems, by combining them. Therefore, the long endurance of an internal combustion engine (ICE) propulsion system during cruise can be achieved, while the higher power demands during take-off and climb can be reached with the help of an EM.

In the context of hybrid propulsion research, one particular energy source that seems to have a lot of potential is hydrogen. This gas has a very high energy density, which makes it attractive as an alternative to fossil fuels. This type of energy source comes across as a more environmentally friendly substitute for fossil fuels, as the product of the reaction with oxygen is just water, and hydrogen can be produced renewably from water as well. However, this type of energy source also present several challenges to its widespread implementation, such as onboard storage. This, and other issues have to be addressed for the use of this fuel in aviation, justifying the importance of further studying these technologies [3].

This work intends to study the application of a FC stack to power an UAV propulsion system, and its integration feasibility in a hybrid electric propulsion

system. There is an existing hybrid propulsion test bench available at the University of Victoria - Centre for Aerospace Research (CfAR). The FC stack apparatus was also available, and the main objective of this research was to integrate and evaluate the FC performance as an energy source for the propulsive system, and test a HEPS making use of the FC.

Following this introductory section, Section 2 presents a brief review of the state of the art for the relevant technologies, while Section 3 describes the components used in the experimental setup. Section 4 explains the different tests performed, and the main results obtained are presented and shortly analyzed. Then, Section 5 explores the possibility of a FC integration in a small UAV. Finally, Section 6 has the concluding remarks of this work.

2. Literature Review

2.1. Hybrid Electric Propulsion

In general, any propulsion system that combines different energy types, including electricity, can be classified as a hybrid electric propulsion system. This first part focuses on aspects that combine an ICE with electrical power, as this is the most relevant power combination to be studied, for UAV applications. Another power source of interest is a FC, which will be discussed later.

Hybrid propulsion systems are an attractive field of study for their promise to take advantage of the strongest points of different power sources, while minimizing their respective drawbacks. Military surveillance missions are an example of this, as electric propulsion is preferred for its lower acoustic and thermal signatures, but without the combination with an ICE its endurance (and range) would be severely limited [4].

Naturally, there are different ways to combine the power sources in a HEPS. The two main distinct configurations are series and parallel, although combinations of the two also exist [5].

In a series configuration, there is no mechanical coupling between the ICE and EM. Instead, a generator connects the two, generating electricity from the ICE mechanical power, and feeding it to the EM powering the propeller (having the option to be stored in a battery). By being mechanically decoupled from the propeller, the ICE can operate freely at its most efficient point. However, the main disadvantages it presents lie in the added mass (having two large electrical machines) and the energy conversion losses [5].

A parallel configuration has the ICE and EM mechanically coupled, allowing for both to drive the propeller at the same time, with their torque being added by the coupling [5]. The mechanical transmission in this configuration is more complex, and the controller design is not as simple, but this configuration can provide mass savings for the system. As the maximum power can be achieved by combining the EM and ICE, they can both be downsized. To address some of the drawbacks of this configuration, particularly the difference in the ideal operating points for the ICE and propeller, a continuously variable transmission (CVT) can be implemented, thus reaching a greater level of freedom selecting the ICE operating point [6].

2.2. Hydrogen Based Propulsion

Making use of hydrogen in aerospace applications is not a new concept. Initially, its low density was used for balloons and airships, over a century ago [7]. For many years, hydrogen has also been used in space applications. Most rocket engines are powered making use of hydrogen as its fuel, using the energy released during its reaction with oxygen to generate the propulsive force [8]. FCs have also been used to generate electric power beginning in the 1960s, with the Gemini and Apollo missions using this technology to generate onboard power. FCs have since become the main energy storage solution for NASA's manned vehicles [9].

Another way to power aircraft making use of hydrogen's high energy density, instead of burning it directly with oxygen, is by making use of fuel cell technology. These systems are more relevant to smaller aircraft, including UAVs.

FCs are similar to traditional batteries, in the sense that they are sources of continuous electric power, generated through a chemical reaction. However, they are open systems, needing a constant input of fuel and oxidizer to generate power. The specific energy of FCs is considerably larger than that of batteries, which addresses one of the main issues in battery usage in UAVs: the weight [3]. FCs can power flight for longer times, covering longer distances, without much increase in weight. For now, however, batteries remain more attractive from an economic point of view, as they have a much lower price than FCs [10].

There are different types of FCs of interest for UAV application, which include Proton Exchange Membrane FC (PEMFC), and Solid Oxide FC (SOFC).

PEMFC It is essentially made up of three parts: anode, cathode, and the proton exchange membrane (PEM), located in between the two sides, allowing protons (H^+) to pass from one side to the other. Each electrode has a porous diffusion layer and a catalyst layer, to facilitate the chemical reactions [11]. Equation 1a occurs in the anode, while equation 1b is in the cathode:

$$H_2 \rightarrow 2H^+ + 2e^-, \tag{1a}$$

$$\frac{1}{2}O_2 + 2H^+ + 2e^- \rightarrow H_2O, \tag{1b}$$

with the overall reaction being simply equation 2:

$$\frac{1}{2}O_2 + H_2 \rightarrow H_2O. \tag{2}$$

While the protons move to the cathode through the PEM, as mentioned, the free electrons movement from

cathode to anode correspond to the electric current. A schematic representation of this process in the the PEMFC is depicted in Figure 1a.

The main advantage PEMFC has over other FCs lies with its comparatively low operating temperature, from 30°C to 110°C. Besides, they are also smaller than the other FCs, and have comparatively high operating efficiency (40∼60%) [12]. However, the main issue of this type of FC is its high cost: the PEM and the catalyst are both expensive [13]. Another issue, common to all types of FCs, is hydrogen storage, which will be discussed below.

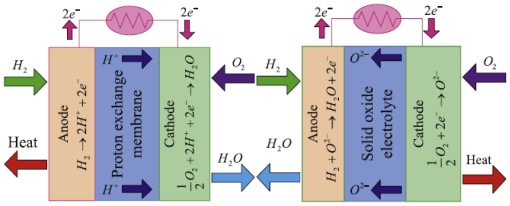

(a) PEMFC; (b) SOFC;

Figure 1: Fuel cell types representation (based on [14]).

SOFC It includes a central solid oxide electrolyte, next to a ceramics porous cathode and anode [15]. It functions in a similar way to the PEMFC, however, instead of protons flowing from the anode to the cathode, it is negative oxygen ions (O^{2-}) that move, in the opposite direction, with its reactions being equation 3a in the anode, and equation 3b in the cathode. The overall reaction is the same as in the PEMFC. However, here the exhaust water is expelled from the anode side. A representation of this type of FC is in Figure 1b.

$$H_2 + O^{2-} \rightarrow H_2O + 2e^-, \tag{3a}$$

$$\frac{1}{2}O_2 + 2e^- \rightarrow O^{2-}, \tag{3b}$$

A SOFC operates at significantly higher temperatures than PEMFC, of up to 1000°C [16]. This can bring some advantages, such as the higher efficiency without using catalysts, but some drawbacks as well, as it requires a thermal management system to handle such high temperatures. Besides, this type of FC can take a long time to start-up, as it warms up to its ideal temperature [17].

Storage Hydrogen, at standard temperature and pressure conditions, has a very low volumetric density of only about 0.09 kg/m^3. Combined with the tight requirements for mass and volume in aircraft, storing this fuel can be a challenge. Possibly the simplest option, is to store it as a compressed gas, increasing its density by submitting it to high pressures, which can be of the order of magnitude of 10 MPa using pressure vessels made of composite materials [18]. These come with a lesser weight penalty than the alternative metal cylinders.

Another option is keeping it in the liquid state, which allows to reach a higher volumetric density than as a compressed gas. However, for hydrogen to be liquefied, temperatures of -253°C need to be reached and maintained. This process comes with great energy losses, about 4 times greater than compressed hydrogen [18]. For storage in these conditions, a highly specialized cryogenic tank is needed.

The final alternative is to chemically bound hydrogen to different elements, creating hydrides. Examples of these compounds include $LiBH_4$ and $NaBH_4$, which have a theoretical hydrogen content of 18.4 wt% and 10.6 wt%, respectively [18]. The main disadvantage of this storage method lies with the need to chemically regenerate the hydrogen, before it can be used, and the need to treat the other byproducts of the reaction. For example, for $NaBH_4$ this reaction is in equation 4:

$$NaBH_4 + 2H_2O \rightarrow NaBO_2 + 4H_2. \tag{4}$$

3. Experimental Setup

In this section the different components that constitute the experimental apparatus used during the testing campaign are described. The PEMFC stack is the main component to be tested, but some peripheral systems are required for its operation.

3.1. Fuel Cell System

The HP 600 fuel cell system (Figure 2a) is an experimental module designed for educational and research purposes, distributed by Heliocentris Energy Systems GmbH [19]. Its core component is the BZ 130 FC stack, produced by Ulmer Brennstoffzellen-Manufaktur GmbH (UBzM). The stack is composed of 24 PEM fuel cells, each with 126 cm^2 of area, and it is rated for a power of 600 W, has an open circuit voltage of 23.5 V, and a maximum current of 45 A. Its recommended operating temperatures are between 45°C and 60°C.

Besides the stack, the system includes the cooling system, that circulates deionized water to regulate the temperature of the stack; the power output system, which allows for the regulated DC and AC outputs of the system; the control panel, where the measured variables could be read and the operating mode changed; and the hydrogen supply circuit, with a flow meter and a pressure regulator, to adjust the inlet pressure to 300 mbar.

The hydrogen supplied to the system came from an external compressed gas cylinder, Praxair's Ultra High Purity 5.0 Hydrogen Cylinder, in Figure 2b. This cylinder stored 99.999% purity hydrogen, at a maximum pressure of 165.5 bar. To be used, its pressure had to be reduced to between 2 and 17 bar by an appropriate regulator (Harris KH1130), also visible in the Figure.

3.2. Electric Load

Some type of electric load had to be connected to the output of the system, which in the first phase of testing was a programmable load, and later different

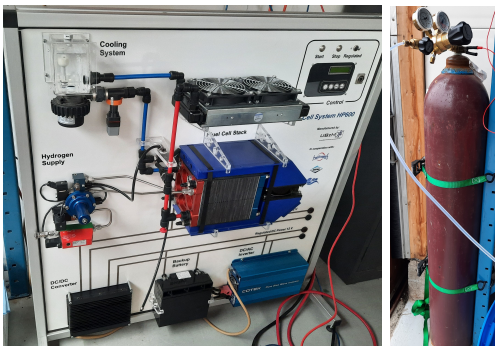

(a) HP 600 FC system. (b) Cylinder.

Figure 2: FC system setup.

electric motors and propellers were used, to simulate a real propulsion application.

The programmable load used was a KIKUSUI PLZ1004WH, in the DC mode. The desired current could be selected on the load, and it would display the values of current, voltage, and power it was consuming from the electric circuit. As for EMs, three different ones were tested: XING2 1404 Toothpick Ultralight Build, E-flite Power 46 BL, AXI 2826/10 Gold Line V2 Long. All three are outrunner brushless DC motors, and were chosen to operate roughly in the same range of voltage and current as the FC could provide. For these motors, two different ESC were used, particularly, a Castle Phoenix Edge HV 120 and a T-Motor Flame 70A LV. They covered the necessary range of voltage and current for the motors tested.

Finally, the EMs were tested while attached to different propellers, which are the components that generate the thrust force when it rotates. For the smaller XING motor, a Nazgul T4030 propeller was used, measuring 10 cm. For the E-flite and AXI motors, a 12"×6 propeller was used.

3.3. Hybrid Test Bench

To test the FC as the power source for a hybrid propulsion system, the hybrid test bench available at CfAR was used. It had been previously developed by different student groups, as part of the continued efforts to study hybrid electric propulsion [20]. This test rig is pictured in Figure 3. It is a parallel hybrid configuration, which had two different EMs to produce the mechanical power that could be combined, namely AXI 5345/16 HD 3D Extreme V2, and AXI 4130/20 Gold Line V2.

Each side of the parallel system is labelled with a different letter, with side A having the larger of the two motors, and are coupled with a rubber band, connected by a unitary gear ratio. Side A also included an electromagnetic clutch, allowing the test operator to connect or disconnect this side at will. This module was connected to the dynamometer (dyno) side of the

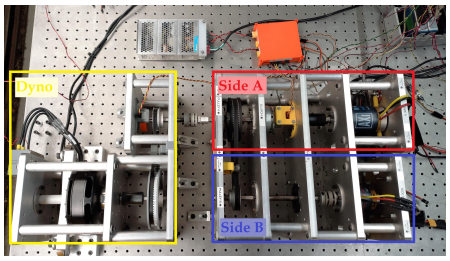

Figure 3: Hybrid test bench.

test bench, centred around the T-Motor U15II KV100, working as a generator, whose power output was converted by a rectifier into a DC signal. The dyno axis was linked to the side A axis by a gear ratio of 2.25, meaning it was rotating 2.25 times slower than the rest of the system.

This setup allows four basic operating modes: side A only, side B only, hybrid, and regeneration mode. The clutch allows the side B only mode to operate truly independent from the side A, while in side A only operation the clutch has to be engaged and, therefore, the motor on the side A has to spin the (unplugged) side B motor. Both other operating modes use the two motors and thus can only work while the clutch is engaged. The test bench included a series of sensors to measure relevant data to characterize its operation, including torque and rotational speed.

4. Tests

Before beginning the experimental campaign, it was necessary to check the condition of each component. In practice, this meant verifying that the different parts of the hydrogen supply circuit were not leaking, and that the HP 600 FC system was functioning correctly. Leak tests were performed in two separate phases: firstly only the hydrogen cylinder, regulator, and hose connections were tested, and only after the hydrogen circuit in the FC system was tested, which had to be done with the system already turned on. As no defects were found, the testing of the stack could commence.

4.1. Fuel Cell Characterization Tests

To characterize the performance of the FC stack, the first test to be performed was a standard polarization curve, to develop a benchmark current-voltage curve of how the FC behaves.

The test consisted in setting the current of the stack, by connecting the programmable load to the unregulated power output, and measuring the corresponding stack voltage. The standard cycle was performed three times, under the same conditions, to confirm the reproducibility of the results. With the data collected directly from the FC system sensors (current and voltage), the power could be easily calculated. Then the values of current and voltage were adjusted per cell, and the current density was calculated, to allow them

to be compared with the manufacturer's data. Using the experimental average of the three tests, this data is presented in Figure 4.

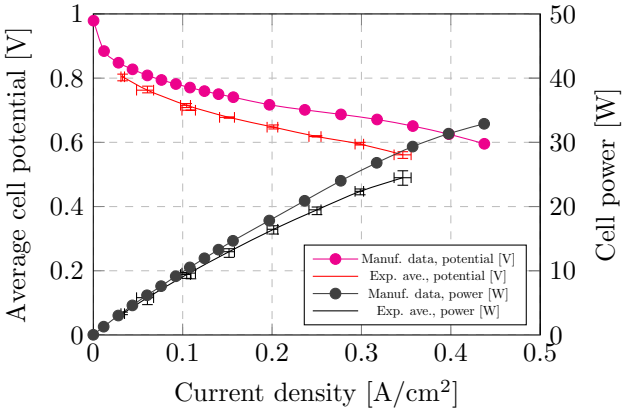

Figure 4: Polarization curve, with experimental average and manufacturer's data.

As can be seen by the small error bars, the results for each of the tests were very similar, confirming that the FC has a predictably behaviour, given the same operating conditions. When comparing this average curve with the manufacturer's data, it can be seen that in reality the average cell potential (and power) is consistently smaller than indicated. This difference is more pronounced at higher currents, being close to 14%, while for the smaller current values this voltage drop is only about 4%.

Despite these differences, the experimental results were in line with the rated power of the FC system as a whole. When the FC was operating at its rated current of 45 A, it was indeed producing 600 W. However, not all that power could be delivered to the external load. Not only were there voltage losses due to resistance in the connections, but also part of the current was being used internally to power the system's electronics. With the correct wiring, as much as 500 W could be reached in the load, over 80% of the total power produced.

Another characterization test that could be completed simultaneously with the previous ones, is the electrical efficiency test. This test is based on equation 5, simplified from [21],

$$\eta_{el} = \frac{U_{stack} \times I_{stack}}{\dot{V}_{hydrogen} \times 179.911446}, \quad (5)$$

where η_{el} it the electrical efficiency of the stack, U_{stack} and I_{stack} are the stack voltage [V] and current [A], respectively, and $\dot{V}_{hydrogen}$ is the hydrogen flow [l/min], all of which could be measured directly by the system's sensors. The result of these calculations, for the three polarization curves performed, are plotted in Figure 5.

Here the measurements were not as close to each other as they were previously for voltage and power.

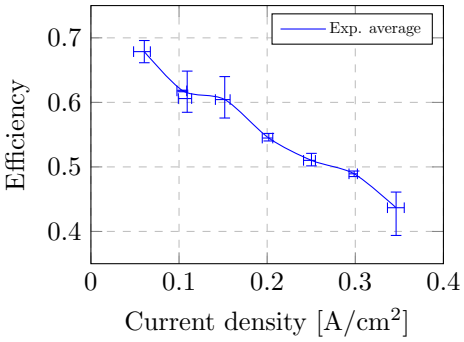

Figure 5: Experimental average for electrical efficiency.

This stems, in part, from the more significant oscillations in the value read by the flow meter sensor, when compared to voltage and current readings. It is also important to take note of the general trend the experimental data shows: higher efficiency for smaller load, reaching values above 60%, and reducing as the current increases, getting close to 40% for the maximum current of the system. This happens because, as the current increases, the different types of voltage losses (activation, ohmic, etc.) become more significant, meaning the FC is not utilizing the entire potential of the hydrogen [22]. Nevertheless, the range of efficiency found is in line what is expected from a PEMFC such as this one [12].

4.2. Propulsion Tests

After the previous tests were completed, it was time to utilize the FC in a propulsion application, using different EMs and propeller, already described. Both LiPo batteries and the FC system were used to power the EMs, so that their performance can be compared. Only static thrust tests were performed, as both the motors and the ambient air around them were at rest.

The tests were performed by installing the EMs in appropriate thrust test stands. The smaller XING motor was tested in the RCbenchmark motor test stand, 1580 series, while the larger EMs were mounted on a larger custom test stand, developed previously at CfAR for this type of propulsion tests. Both setups measured the electrical power feeding the EM, giving voltage and current readings, as well as the thrust force and torque being applied in the test stand. This data, along with time, was logged and saved in spreadsheet format, for better analysis.

Figure 6 show the thrust measured, as a function of the throttle setting, for each of the EMs tested. It is important to notice that while the XING motor presents positive values of thrust, the other two show negative values (the axis direction is flipped for ease of visualization) as the propeller was installed in a pusher configuration, for safety reasons.

The three plots show a similar behaviour: the thrust

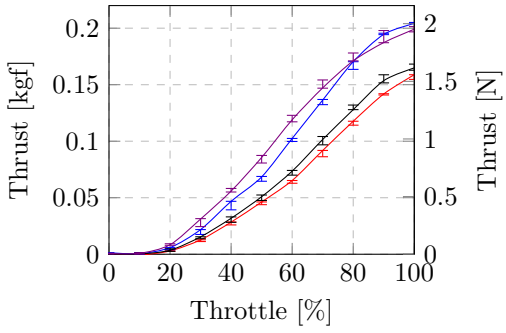

(a) XING2 1404.

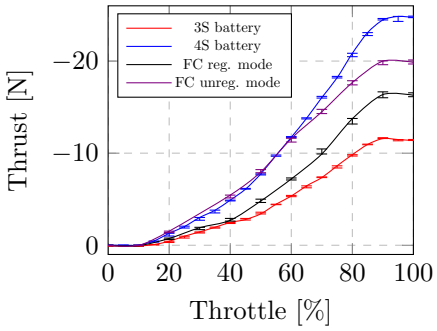

(b) E-flite 46.

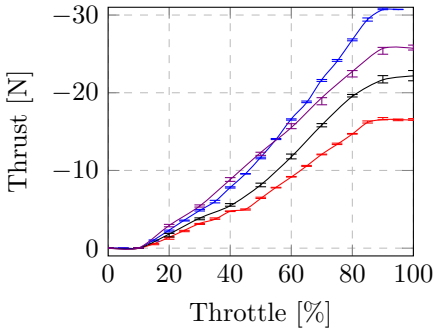

(c) AXI 2826/10 Long V2.

Figure 6: Thrust tests.

generated when connected to the regulated power mode is in-between the performance for the 3S and 4S batteries; while the unregulated power mode produces results that begin above the ones from the 4S battery, but a lower thrust is generated for the highest throttle settings. This behaviour can essentially be explained by the difference in voltage each power source is able to provide, since the voltage supplied to an EM is essentially related to its rotational speed, which, in turn, reflects on the torque necessary to spin it, and the thrust it generates. To visualize this voltage being supplied to the EMs, an example is shown in Figure 7, using data from the E-flite motor, which is in line with the other EMs.

It can be observed that both batteries and the regulated power mode of the FC show little variation in their voltage, with voltage drops of about 0.5 to 1 V. On the other hand, the unregulated power mode had

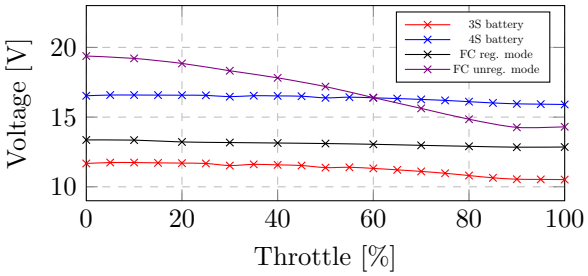

Figure 7: Voltage supplied to the E-flite motor.

a much greater voltage variation throughout the test, dropping 5.1 V as the load increased. The difference in the behaviour of the FC system's two modes are justified by the way they operate. In the regulated power mode, the load is in parallel with the backup battery of the system, ensuring low voltage variation. As its voltage (∼13 V) is in-between those of the two batteries, it is explained why the thrust observed with the regulated mode was higher than the one using the 3S battery, but still below that of the 4S battery. In the case of the unregulated output mode of the system, the electric load is connected directly to the terminals of the FC stack. As seen from the polarization curve, it has quite a significant voltage drop over its operating range. For the lower load, it has a voltage above the 4S battery, and thus, a higher thrust too, but the stack voltage drops below the 4S battery at 60% throttle, which is, as expected, the point in Fig. 6b where both thrust curves intersect.

Even in the unregulated power mode, the voltage and current of the stack are not exactly the same as the ones being supplied to the EMs. As discussed previously, there are losses, and current being consumed internally by the system. The voltage felt by the EMs was about 0.5 V lower than the stack's voltage, and the current was around 5 to 6 A lower. Still, the AXI 2826 motor consumed over 500 W of power at full throttle, which had been observed as the maximum that could be provided to an electrical load connected to the FC.

4.3. Hybrid Tests

Following the propulsion tests, the FC stack was tested as a power source to the hybrid test bench described above. The FC system was connected to the side B of the test bench, where the smaller AXI motor was installed, using the unregulated operating mode. Side A was powered using two 6S batteries, connected in series, corresponding to a 12S battery, while the programmable load was used to dissipate the power generated by the dyno.

In the first couple of tests conducted, there was no load demand by the programmable load. Therefore, all the power supplied to the system was dissipated mechanically, with no electrical generation by the dyno. This power was the necessary to overcome the rota-

tional friction between the different components, as well as the power dissipated on the EMs' coils. The power, hybridization degree, and RPM measured are shown in Figure 8. The hybridization degree was defined as the ratio between the side B electrical power (from just the FC) and the total electrical power supplied to the system.

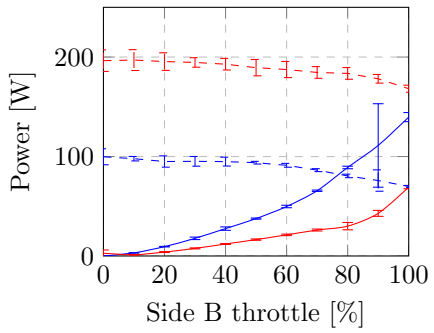

(a) Sides A (dashed) and B (solid) power.

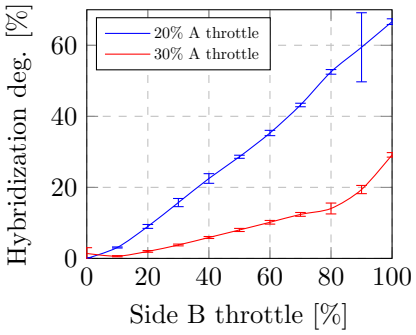

(b) Hybridization degree.

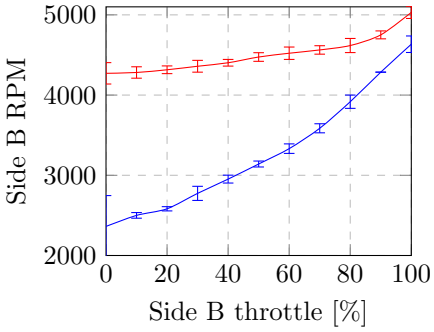

(c) RPM.

Figure 8: Test bench variables for the unloaded hybrid tests.

Unlike the following tests, the side A throttle was not increased beyond 30% when the system was unloaded, because the degree of hybridization was already quite low, only at around 30%. Increasing the side A throttle even further would only reduce the overall influence of side B.

Nevertheless, the overall system behaviour can be analyzed. With the increase in throttle, for either motor, there was an associated increase in the system's RPM, as more average voltage was being supplied to the EMs. This, in turn, came with and increase in the power consumed by each motor. For each side A throttle setting, however, the power being consumed decreased when the side B throttle was increased, since more of the power needs of the system were being met by the side B EM. This translates to the increase in the hybridization degree with the side B throttle seen.

While this general behaviour is observed for both tests, it becomes less pronounced when the side A throttle setting was increased. Given the larger size of the side A motor, and the much higher voltage it was being supplied with, it is natural that, as it was generating more power, the whole system became less sensitive to variation in the smaller (and undervoltaged) side B motor.

Following these unloaded tests, the programmable load was set to 5 A first, and then increased to 10 A. The same variables as previously, but now for this second loaded case, are in Figure 9. In this data, the same trends observed before are present. No tests were performed beyond 40% side A throttle, as the side B influence on the system would further decrease, and to avoid overspinning side B.

When compared with the unloaded tests, the increase in the load changes the system's behaviour in predictable ways. Firstly, the power necessary to rotate the system increases, for the same throttle settings. As in these tests the dyno motor was functioning as a generator, the greater torque necessary to rotate the system translated to a decrease of several hundred RPM for the whole system. With the increase in power demand, there was a larger share of it being drawn from side B, leading to an increase in the hybridization degree, which reached the largest value observed, with nearly 76% for the 20% side A throttle test.

Besides the test bench variables, the FC behaviour can also be analyzed, and compared to the previous benchmark performance. With that goal, the plot from Figure 10 is included, which shows the FC's voltage and current for the previous tests, in the order they were performed. The 5 A loaded tests were performed between the two sets of tests analyzed in this document, but are not included in this plot, to simplify it.

Here, it must be noticed the considerably lower voltage observed in these hybrid tests, when compared to the polarization curve previously determined. This points to an important equipment limitation, which affected the initial conditions in which each test was conducted: the programmable load was used for the hybrid test bench and could not be connected to the FC stack in-between tests to warm it up. Given the relatively low current being drawn, the temperature of the stack steadily decreased throughout the tests, from 47.8°C (already below the benchmark 55°C), to almost 40°C, well below the lower operating temperature limit given by the manufacturer (45°C).

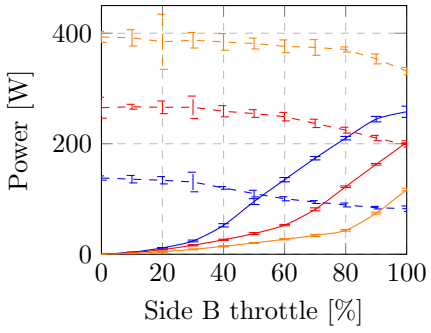

(a) Sides A (dashed) and B (solid) power.

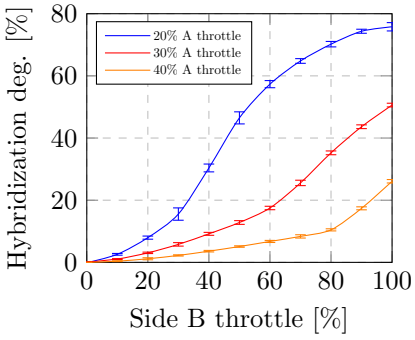

(b) Hybridization degree.

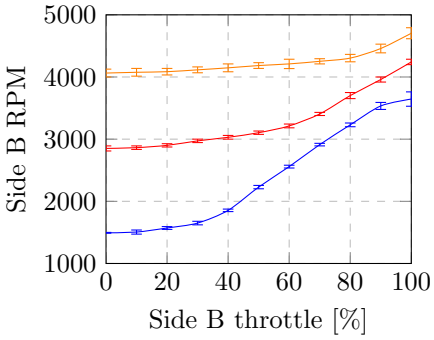

(c) RPM.

Figure 9: Test bench variables for the loaded 10 A hybrid tests.

The voltage difference between the curves reaches about 0.8 V of difference for the largest current observed. While this may represent only about 5% of the total voltage of the FC, it is still a much higher variation in performance than what was observed when the FC was operating at a consistent temperature. This behaviour points to the need for a better thermal management strategy, possibly with some heating system, alongside the existing cooling system, to ensure the correct FC performance.

5. Application to an UAV

As with any propulsion system, the final goal is aircraft integration, in the case of this project, in UAVs. The first thing to consider is for which aircraft this propulsion system would be designed for, so, as a reference, the *Mini-E* aircraft, developed at CfAR, will be used, whose propulsion system sizing was done by Sara Pedro [23].

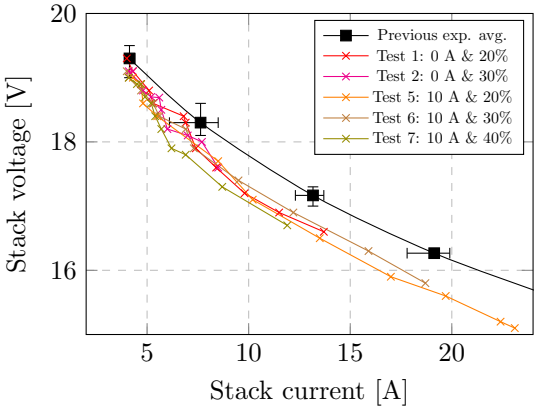

Figure 10: Fuel cell current-voltage behaviour during the hybrid tests.

This is a small electric vertical take-off and landing (VTOL) UAV, with a maximum take-off mass of 7 kg, with around 0.45 kg of battery mass, and power requirements of about 100 W for cruise, 440 W for dash, and 1000 W for VTOL. Immediately, incompatibilities between the FC at hand and the UAV requirements can be noticed. Mainly, the FC used is far too heavy to be used in flight, with just the stack weighing 9.8 kg. The hydrogen storage solution used is also not appropriate for flight: it has a mass of over 65 kg, with the hydrogen stored inside accounting for less than 1% of the total.

However, while this indicates that the setup tested is not suitable for an UAV integration, this should not be taken as an impossibility to utilize FC technology as the basis of a propulsion system. Simply, the FC system available was never designed for such an application, being intended for educational purposes, in a classroom or lab. The hydrogen storage choice was also made based on the availability of the compressed gas cylinder, and only with ground testing in mind, knowing that such a heavy metal cylinder was not what would be used in an eventual UAV integration.

With this in mind, some options available in the market were investigated, of which two stand out: Intelligent Energy's IE-SOAR 800W Second Generation [24], and H3 Dynamics' Aerostak A-250 [25], with the characteristics compiled in Table 1.

Table 1: Specifications for two commercially available FCs.

FC	IE-SOAR	Aerostak
Rated Power [W]	800	250
Peak Power [W]	2400	300
Weight [kg]	1.45	0.72

While these stacks cannot accommodate, in continuous power, all the flight segments of the UAV, a propulsion system with a FC is likely going to include at least one battery, which can make up for the extra power needed during take-off and climb. Given that, the Aerostak's reduced mass makes it a very attractive option given the mass constraints of such a small UAV. Otherwise, the IE-SOAR, with about double the mass but more than three times the power output, could fully cover the power demand during dash, and could supply the majority of power for VTOL, requiring less backup battery capacity. Estimating the battery mass necessary to cover the energy requirements during take-off the same way Sara Pedro did for the entire flight, masses of 0.85 kg and 1.5 kg were found for the FC-battery hybrid, using the Aerostak and the IE-SOAR, respectively.

Another mass penalty to the propulsion system will come from the hydrogen storage. As the simplest solution, similar to what was used in the tests performed, some compressed gas cylinders were analyzed, particularly the ones from H3 Dynamics [26]. Its A5 model, for example, weighs only 1.65 kg, and can store 120 g of hydrogen, for an energy density of 2.42 kWh/kg, much higher than batteries (170.33 Wh/kg). When including the pressure regulator, the total mass penalty can be between 2 and 3 kg, depending on the FC chosen, when compared to the 0.45 kg estimation of battery mass.

However, this integration would have associated benefits mainly in the form of extended endurance. To estimate it, the cruise flight phase was considered, as it is where most of the hydrogen's stored energy would be used. For the Aerostak the maximum hydrogen consumption is 2.8 L/min. Calculating for 95% of the hydrogen being used, with the FC operating in maximum power conditions, the A5 cylinder could potentially fly 452 min (7.5 h). For the IE-SOAR stack the manufacturer provides some integration example values for UAV endurance: with a 5 L cylinder, and total system mass of 3.9 kg (in line with the value reached here) a flight time of 4.9 hours was given. These rough estimations can indicate the scale at which an UAV endurance can be extended by using a FC as part of its propulsion system, given its battery-only endurance of 20 min cruise.

6. Conclusions

The main goal of this research project was to study the usage of FC technology with the purpose of UAV propulsion in mind. Several steps had to be taken, from studying some of the theoretical background for the technology used, to getting acquainted with the experimental setup and performing several different tests.

The propulsion tests results showed some promise for FC-powered propulsion for small UAV, as they confirmed that a FC can correctly power an EM and propeller, like the ones found on small UAV. Moreover, the hybrid tests showed that the FC was able to significantly reduce the power drawn on the side A, without changing the system loading or the side A settings. This dynamic power splitting shows promise in lessening fuel consumption in a possible FC–ICE configuration. Finally, the possibility of UAV integration was briefly analyzed, highlighting what benefits and challenges exist when applying this technology to small UAV.

References

[1] Airbus. *Airbus Global Market Forecast 2021-2040*. https://www.airbus.com/sites/g/files/jlcbta136/files/2021-11/Airbus-Global-Market-Forecast-2021-2040.pdf. Last accessed on 11.05.2022. 2021.

[2] R. Sims et al. "Climate Change 2014: Mitigation of Climate Change. Contribution of Working Group III to the Fifth Assessment Report of the Intergovernmental Panel on Climate Change". In: ed. by O. Edenhofer et al. Cambridge, United Kingdom and New York, NY, USA: Cambridge University Press, 2014. Chap. Transport.

[3] Z.F. Pan, L. An, and C.Y. Wen. "Recent advances in fuel cells based propulsion systems for unmanned aerial vehicles". In: *Applied Energy* 240 (2019), pp. 473–485. DOI: 10.1016/j.apenergy.2019.02.079.

[4] T. A. Rotramel. *Optimization of Hybrid-Electric Propulsion Systems for Small Remotely-Piloted Aircraft*. Master's thesis, Air Force Institute of Technology. Nov. 2011.

[5] J. Schömann. *Hybrid-Electric Propulsion Systems for Small Unmanned Aircraft*. PhD Thesis, Technische Unisersität München. July 2014.

[6] C. J. Brace et al. "An operating point optimizer for the design and calibration of an integrated diesel/continuously variable transmission powertrain". In: *Proceedings of the Institution of Mechanical Engineers, Part D: Journal of Automobile Engineering* 213 (1999), pp. 215–226. DOI: 10.1243/0954407991526810.

[7] D. Cecere, E. Giacomazzi, and A. Ingenito. "A review on hydrogen industrial aerospace applications". In: *International Journal of Hydrogen Energy* 39.20 (2014), pp. 10731–10747. DOI: 10.1016/j.ijhydene.2014.04.126.

[8] National Aeronautics and Space Administration. *Space Applications of Hydrogen and Fuel Cells*. https://www.nasa.gov/content/space-applications-of-hydrogen-and-fuel-cells. Last accessed on 19.05.2022.

[9] K. A. Burke. *Fuel Cells For Space Science Applications*. https://ntrs.nasa.gov/api/citations/20040010319/downloads/20040010319.pdf. Last accessed on 19.05.2022. Nov. 2003.

[10] N. Belmonte et al. "Fuel cell powered octocopter for inspection of mobile cranes: Design, cost analysis and environmental impacts". In: *Applied Energy* 215 (2018), pp. 556–565. DOI: 10.1016/j.apenergy.2018.02.072.

[11] X. Cheng et al. "A review of PEM hydrogen fuel cell contamination: Impacts, mechanisms, and mitigation". In: *Journal of Power Sources* 165.2 (2007). IBA – HBC 2006, pp. 739–756. DOI: 10.1016/j.jpowsour.2006.12.012.

[12] A. Gong and D. Verstraete. "Fuel cell propulsion in small fixed-wing unmanned aerial vehicles: Current status and research needs". In: *International Journal of Hydrogen Energy* 42.33 (2017), pp. 21311–21333. DOI: 10.1016/j.ijhydene.2017.06.148.

[13] A.B. Bose and X. Zhu. "Design of stable and durable polymer electrolyte membrane fuel cells by embedding hydrophobic cage-structured material in cell components". In: *Fuel* 235 (2019), pp. 954–961. DOI: 10.1016/j.fuel.2018.08.051.

[14] B. Wang et al. "Current technologies and challenges of applying fuel cell hybrid propulsion systems in unmanned aerial vehicles". In: *Progress in Aerospace Sciences* 116 (2020), p. 100620. DOI: 10.1016/j.paerosci.2020.100620.

[15] A. M. Abdalla et al. "Nanomaterials for solid oxide fuel cells: A review". In: *Renewable and Sustainable Energy Reviews* 82 (2018), pp. 353–368. DOI: 10.1016/j.rser.2017.09.046.

[16] Z. Ji et al. "Thermodynamic analysis of a solid oxide fuel cell jet hybrid engine for long-endurance unmanned air vehicles". In: *Energy Conversion and Management* 183 (2019), pp. 50–64. DOI: 10.1016/j.enconman.2018.12.076.

[17] M.D. Fernandes et al. "SOFC-APU systems for aircraft: A review". In: *International Journal of Hydrogen Energy* 43.33 (2018), pp. 16311–16333. DOI: 10.1016/j.ijhydene.2018.07.004.

[18] H. Barthelemy, M. Weber, and F. Barbier. "Hydrogen storage: Recent improvements and industrial perspectives". In: *International Journal of Hydrogen Energy* 42.11 (2016). Special issue on The 6th International Conference on Hydrogen Safety (ICHS 2015), 19-21 October 2015, Yokohama, Japan, pp. 7254–7262. DOI: 10.1016/j.ijhydene.2016.03.178.

[19] Heliocentris Energy Systems GmbH. *Operation Guide - HP 600 Fuel Cell System*. third edition, January 2008.

[20] L. Machado, J. Matlock, and A. Suleman. "Experimental evaluation of a hybrid electric propulsion system for small UAVs". In: *Aircraft Engineering and Aerospace Technology* 92.5 (2019), pp. 727–736. DOI: https://doi.org/10.1108/AEAT-06-2019-0120. URL: https://www.emerald.com/insight/content/doi/10.1108/AEAT-06-2019-0120/full/html.

[21] M. Råberg-Hellsing and C. Kaijser. *Specification of Test Procedures for Polymer Electrolyte Fuel Cell Stacks*. June 2004.

[22] M. H. Nehrir and C. Wang. *Modeling and Control of Fuel Cells: Distributed Generation Applications*. John Wiley & Sons, Inc., 2009.

[23] S. de Almeida Pedro. *Sizing and Integration of an Electric Propulsion System for a VTOL UAV*. Marter's thesis, Instituto Superior Técnico. Dec. 2020.

[24] Intelligent Energy. *IE-SOAR 800W second generation*. https://www.intelligent-energy.com/wp-content/uploads/2022/09/ie-soar-800w-gen2.pdf. Last accessed on 13.10.2022.

[25] H3 Dynamics. *Hydrogen Fuel Cell Systems by H3 Dynamics — Super Lighweight and Power Dense For Air Mobility Needs*. https://www.h3dynamics.com/hydrogen-fuel-cell-systems-for-air-mobility. Last accessed on 13.10.2022.

[26] H3 Dynamics. *H3D Brochure Complete 2022 V8*. https://www.h3dynamics.com/_files/ugd/3029f7_db7f1517df744509b837916c4d939ae3.pdf. Last accessed on 17.10.2022. 2022.